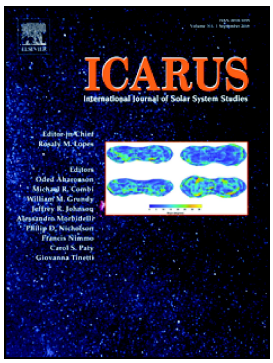

Simulating the diffusion of hydrogen in amorphous silicates: A 'jumping' migration process and its implications for solar wind implanted lunar volatiles

Liam S. Morrissey, D. Pratt, W.M. Farrell, O.J. Tucker, S. Nakhla, R.M. Killen

PII: S0019-1035(22)00096-3

DOI: https://doi.org/10.1016/j.icarus.2022.114979

Reference: YICAR 114979

To appear in: *Icarus*

Received date: 7 September 2021

Revised date: 28 February 2022

Accepted date: 3 March 2022

Please cite this article as: L.S. Morrissey, D. Pratt, W.M. Farrell, et al., Simulating the diffusion of hydrogen in amorphous silicates: A 'jumping' migration process and its implications for solar wind implanted lunar volatiles, *Icarus* (2021), https://doi.org/10.1016/j.icarus.2022.114979

Simulating the Diffusion of Hydrogen in Amorphous Silicates: A 'Jumping' Migration Process and its Implications for Solar Wind Implanted Lunar Volatiles

Authors: Liam S. Morrissey[1,2 a)], J. Pratt[3], W.M. Farrell[1], O.J. Tucker[1], S. Nakhla[3], R.M. Killen[1]

Affiliations:

[1] NASA Goddard Space Flight Center, 20771, Greenbelt, Maryland, United States

[2] Catholic University /CRESST II, 200005, Washington, DC, 20005, United States

[3] Department of Mechanical Engineering, Memorial University of Newfoundland, A1C 5S7, St. John's, Newfoundland & Labrador, Canada

a) Corresponding author: Liam Morrissey (lsm088@mun.ca)

1 Abstract

We use molecular dynamics (MD) simulations to better explain the movement of atomic hydrogen in amorphous silica and quantify the planetary science implications of these findings. Previous MD simulations had a large range of predicted values and did not agree well with experiment. Our simulations sample atomic motion for a longer duration and consider a wider range of temperatures than previous simulations. In contrast to constant atomic motion, the hydrogen atoms were shown to undergo random intermittent jumps from one oxygen atom to another, the number of which increase with temperature. Predicted diffusion coefficients had a better agreement to experimental values than previous MD simulations, suggesting the importance of longer simulation durations for better statistics. The low activation energy and jumps observed at lunar temperatures do not support the theory of diurnal variations in OH content for an undamaged amorphous silica surface. Instead, we conclude that energetic solar wind impacts can induce two competing atomic hydrogen motion processes in the exposed surface: A prompt effect that induces jumps in the temperature spike volume, but also a long-term effect of damage in the structure that traps atomic hydrogen. We then use SDTrimSP to quantify the damage created during exposure and MD to demonstrate the H retention and trapping near these defects. Damage was shown to be dependent on impact energy, with defects easily retaining implanted hydrogen. MD results like those presented herein on unweathered surfaces are therefore most relevant to magnetic anomalies. As a result, we demonstrate the importance of lunar volatile models to account for the damage state of the substrate when modelling hydrogen diffusion, retention, and subsequent OH/water production.

Keywords: Moon, surface; Solar Wind

1 Introduction

One of the most important processes in our solar system is the interaction of the solar wind (SW) with planetary surfaces. The SW is a stream of high-energy charged particles originating from the sun consisting of electrons, protons, helium and trace amounts of heavy ions such as oxygen and iron (Von Steiger et al. 2000). These trace heavy ions are in higher proportion for the high energy tails (Von Steiger et al. 2000; Killen et al. 2012; Nénon & Poppe 2020). The Moon does not possess a significant atmosphere or intrinsic magnetic field to shield from the SW; its surface is therefore constantly bombarded by SW particles and ions from Earth's magnetosphere when orbiting in the geomagnetic tail. This ion-surface interaction is critical to the evolution of the surface and exospheric composition of bodies such as the Moon and Mercury (Elphic et al. 1991; Killen & Ip 1999; Kallio et al. 2019). Specifically, observations of widespread lunar hydroxyl and water across the lunar surface and H_2 and H_2O in the exosphere indicate that the SW-surface interaction is an important component to the lunar hydrogen cycle (Pieters et al. 2009; Schultz et al. 2010; McCord et al. 2011; Stern et al. 2013; Benna et al. 2019). The first definitive evidence of excess lunar hydrogen came from neutron spectroscopy (Feldman et al. 1998), which was then later confirmed in lunar rocks by Saal et al. (2008). As predicted much earlier (Zeller et al. 1966; Mattern et al. 1976), Pieters et al. (2009), Sunshine et al. (2009) and Clark (2009), discovered a widespread OH veneer was by examining IR reflectance spectra obtained from the Moon Mineralogy Mapper on Chandrayaan-1. This research suggested the possibility of water creation via an OH combinative reaction. Further research suggested that SW atomic hydrogen (H) implantation and retention was a likely source of this OH veneer (Starukhina & Shkuratov 2000; Starukhina 2006; McCord et al. 2011). As high

energy hydrogen impacts the lunar surface it can diffuse and chemically react with oxygen in the silicate based regolith to form water products (Starukhina & Shkuratov 2000; Starukhina 2006; McCord et al. 2011). Based on these observations, Farrell et al. (2017) used a statistical mechanics approach to study the outgassing and implantation of atomic hydrogen from the SW in SiO_2. Their study demonstrated the importance of the implantation depth, temperature, and distribution of activation energies on atomic hydrogen diffusion. This study concluded that a better understanding of atomic hydrogen retention and diffusion mechanisms in the lunar surface was needed to further understand the production of OH and H_2O from the SW.

Statistical based approaches to modelling hydrogen implantation and diffusion employ a range of activation energies and diffusion coefficients sparsely constrained by observations and laboratory experiment. However, the atomic-level mechanism of diffusion has not been investigated in detail, and it is one important constraint on the production of hydrogenated products within regolith grains (Farrell et al. 2017). Similarly, experiments typically measure the diffusion coefficient and cannot provide information on the actual diffusion mechanism (Fink et al. 1995). For example, Fink et al. (1995) and references within compiled a large set of diffusion coefficients for hydrogen within various silica crystalline arrangements. While a range of diffusion coefficients was observed, the reason for this range and the subsequent diffusion mechanisms were not revealed at the atomic level. Consequently, molecular dynamics (MD) simulations are often used to probe the inter-lattice diffusion on the atomistic scale (Fogarty et al. 2010; Sheikholeslam et al. 2016). For example, Sheikholeslam et al. (2016) modelled atomic hydrogen diffusion in amorphous SiO_2 and predicted a diffusion coefficient of 10^{-11} cm^2/s at 650

K. In contrast, Fogarty et al. (2010) considered a nearly identical system and predicted a diffusion coefficient $1.7x10^{-6}$ cm^2/s at 300 K, five orders of magnitude higher than Sheikholeslam et al. Given that diffusion is known to increase with temperature (Fink et al. 1995), the temperature difference cannot explain the large differences found in the models. Therefore, currently there are significant discrepancies in predicted hydrogen diffusion coefficients obtained using MD. These values were also highly discrepant when compared to experimental diffusion coefficients for atomic hydrogen in amorphous silica, $1x10^{-7}$ cm^2/s (Fink et al. 1995). Given that the same interatomic force field was used in both studies, this suggests a potential issue with the methodology for tracking diffusion coefficients in silicates. Correspondingly, there was also a large range of simulated and measured activation energies for atomic hydrogen diffusion in silica (0.05-0.9 eV), emphasizing the need for closer investigation (Fink et al. 1995; Fogarty et al. 2010; Sheikholeslam et al. 2016). Finally, previous experiments and simulations have considered only a limited range of temperatures and again do not discuss the actual mechanisms of diffusion. The purpose of this study is to examine the atomistic scale mechanisms of hydrogen diffusion in amorphous silica over a range of temperatures relevant for the Moon. Diffusion is affected by a myriad of properties and processes such as composition, space weathering, solar heating and more. To this end, as a baseline for comparison, in this initial study we examine the effect of temperature and defects on the atomic motion of hydrogen in amorphous SiO_2. The chemical production of hydrogenated products in the regolith such as H_2O, OH and H_2 will depend on this diffusive motion.

2 Methodology

2.1 Interatomic Potential and Simulation Details

MD is a deterministic numerical method used to simulate the movement of atoms and molecules within a substrate. Simulations begin with the initial positions and velocities of all atoms defined within the system based on the crystallinity and/or crystal orientation of the substrate. An interatomic potential is used to define forces between interacting atoms and thus calculate the atomic accelerations. Finally, Newton's equations of motion are used to predict the next set of positions and velocities incremented by a prescribed timestep. Simulations of diffusion within silicates require an interatomic potential capable of modelling the dynamic bond formations and energies as a function of time and temperature. As such, atomic interactions during diffusion simulations were modelled using a reactive force field (ReaxFF) interatomic potential as implemented by the Large-Scale Atomic/Molecular Massively Parallel Simulator (LAMMPS), a commonly used MD program from Sandia National Laboratories (Plimpton 1995; Van Duin et al. 2001).

ReaxFF is a bond-order based force field that can describe both bond breaking and formation [10]. What makes ReaxFF unique is its ability to dynamically model interactions that are both connected and non-bonded. First, connectivity dependant reactions (valence and torsion energy) are modelled such that when bonds are broken their energy is eliminated. Second, non-bonded interactions, van der Waals and Coulomb, are calculated regardless of connectivity between every atom pair in the set-up. These distance dependent interactions are updated at every simulation step, allowing for bonds to both break and form. As a result of this

combination, ReaxFF can describe both covalent and metallic systems. More detail on the ReaxFF method can be found in van Duin et al. (2001). Specifically, we used a SiOH potential that was originally developed to describe hydrogen-silica interactions and has been previously used to simulate hydrogen diffusion (Fogarty et al. 2010; Sheikholeslam et al. 2016).

2.2 Preparing Amorphous Silica

Lunar soils primarily contain a combination various silicates including olivine $(Mg,Fe)_2SiO_4$, pyroxene $(Ca,Mg,Fe)SiO_3$ and plagioclase felspars (Williams & Jadwick 1980). Si and O are the two most abundant components within these species and typically occur in the form of silica (SiO_2) with wt. % ~ 45 (McKay et al. 1991). Therefore, while pure SiO_2 may not be present in high abundance on the lunar surface, it remains relevant for olivine and pyroxene based surfaces. For baseline comparisons with relevant lunar research (Farrell et al. 2015; Jones et al. 2018; Tucker et al. 2019), we conducted simulations of hydrogen in amorphous silica. We began by constructing an amorphous silica substrate with mass density consistent with experimental results (Haynes 2014). First 2000 silica molecules were placed randomly in a 67 x 67 x 20 $Å^3$ simulation box with an initial density of 2.2 g/cm^3. Boundary conditions were periodic in the x, y, z directions to eliminate edge effects and simulate an essentially infinite bulk. Following previous similar simulations (Fogarty et al. 2010; Sheikholeslam et al. 2016), the system temperature was then increased to 4000 K and cooled back to 300 K using a Nose-Hoover thermostat with an NVT (particles, volume, temperature) ensemble that keeps the volume and number of particles fixed while allowing the temperature to change for 150 ps. Next, the system was again heated to 4000 K in an isobaric-isothermal NPT (number of particles, pressure, temperature) ensemble that fixed the number of particles while allowing

the volume to change based on the desired temperature and pressure held at that temperature for 75 ps. Finally, the system was cooled back down to 300 K using an NPT ensemble with a cooling rate of 10^{14} K/s resulting in an equilibrated amorphous silica structure. Silica structural properties have been previously shown to be independent of cooling rate below 10^{15}K/s (Sheikholeslam et al. 2016). After 225 ps this equilibration process resulted in a density of 2.11 g/cm^3, agreeing well with experimental results, 2.2 g/cm (Haynes 2014). This density check indicated the starting amorphous sample was suitable.

2.3 Calculating Diffusion and Activation Energy

After preparation the amorphous silica substrate was then heated/cooled in an NPT and then NVT ensemble as described above for 50 ps each to the desired simulated temperature (100 K, 300 K, 450 K, 600 K, 800 K, 1000 K, 1500 K). This range of temperatures was selected to better examine the effect of temperature on diffusion for a range of planetary and lunar relevant values. For example, while lunar surface temperatures will not reach the high end of this range, short-term temperature spikes within the substrate due to SW or micrometeorite bombardment may be an important driver of subsurface diffusion (Anders & Urbassek 2017). Following previous studies (Farrell et al. 2015; Tucker et al. 2019), we have assumed SW deposited H ions will be neutralized within the surface. As such, 30 atomic hydrogen neutrals were placed randomly throughout the structure such that there was no interaction or overlap between hydrogen atoms. Finally, the silica-hydrogen system was then held at each temperature in an NVT ensemble for 2000ps, ten times longer than previous similar simulations (Sheikholeslam et al. 2016). Consistent with previous MD studies (Fogarty et al. 2010; Sheikholeslam et al. 2016), the pressure for all boundaries in NPT ensembles was kept to 1 atm

to ensure pressure gradients at the boundary did not influence diffusion. The simulation timestep was 0.0005 ps, a commonly used timestep for diffusion simulations with ReaxFF potentials.

Diffusion of the hydrogen atoms was first tracked throughout the simulation using the mean square displacement (MSD) following similar MD studies (Sheikholeslam et al. 2016) using equation 1:

$$\mathrm{MSD} = \langle |\bar{\mathbf{r}}(\mathrm{t} + \mathrm{t}_0) - \bar{\mathrm{r}}(\mathrm{t})|^2 \rangle \qquad \text{Equation 1}$$

where $\bar{\mathbf{r}}(t)$ is the position of the atom. For each temperature the average MSD was calculated in 200 ps intervals from 50-2000 ps. Then the diffusion coefficient (D) was calculated using the Einstein relationship as per equation 2:

$$\mathrm{D(T)} = \frac{1}{6\mathrm{Nt}_0}\mathrm{MSD}_{\mathrm{avg}} \qquad \text{Equation 2}$$

Where N is the number of hydrogen atoms (30) and $\mathrm{MSD}_{\mathrm{avg}}$ is the average MSD. Finally, the activation energy was calculated using the slope of an Arrhenius plot for the temperature ranges simulated. As such, because of the scale and lack of grain boundaries in the amorphous substrate, diffusion in this paper is relevant to movement within the crystal lattice of an individual grain. We differentiate this internal diffusion from inter-grain molecular transport, which is referred to as Knudsen diffusion. Knudsen diffusion represents repeated surface

adsorption/desorption 'hops' of the molecule in porous material (Sarantos & Tsavachidis 2020), as opposed to internal atomic migration.

The simulation duration of 2000 ps was verified by testing the diffusion coefficient at a low (300 K) and intermediate temperature (800 K) and observing less than a 5% change in diffusion coefficient for a 50% increase in simulation time. Each simulation took several days on Compute Canada, a cluster-based computing service.

3 Results

3.1 Simulated Diffusion Coefficient and Activation Energies

As shown in Figure 1, MD simulations were used to calculate diffusion coefficients as a function of temperature between 100-1500 K (A). With increasing temperature there is an increase in the diffusion coefficient of atomic H. As seen in the Arrhenius plot in Figure 1, there is not a clear linear behavior across the entire temperature regime (R-squared = 0.89). This has been observed in previous MD studies, where it was instead suggested that there were multiple activation energy regions (Zhai et al. 2012; Sheikholeslam et al. 2016). In the first region (R-squared = 0.99), between 100-450 K, diffusion coefficients are low, and the linear behavior corresponds to an activation energy of 0.02 eV. Between 650-1500 K a second linear region exists (R-squared = 0.96) where there is a noticeable increase in the slope, corresponding to a higher activation energy of 0.09 eV. However, the physical meaning behind these two regions is unclear. For example, Sheikholeslam et al. concluded that low hydrogen activation energy regions in amorphous SiO_2 corresponded to lattice vibrations as opposed to actual diffusion.

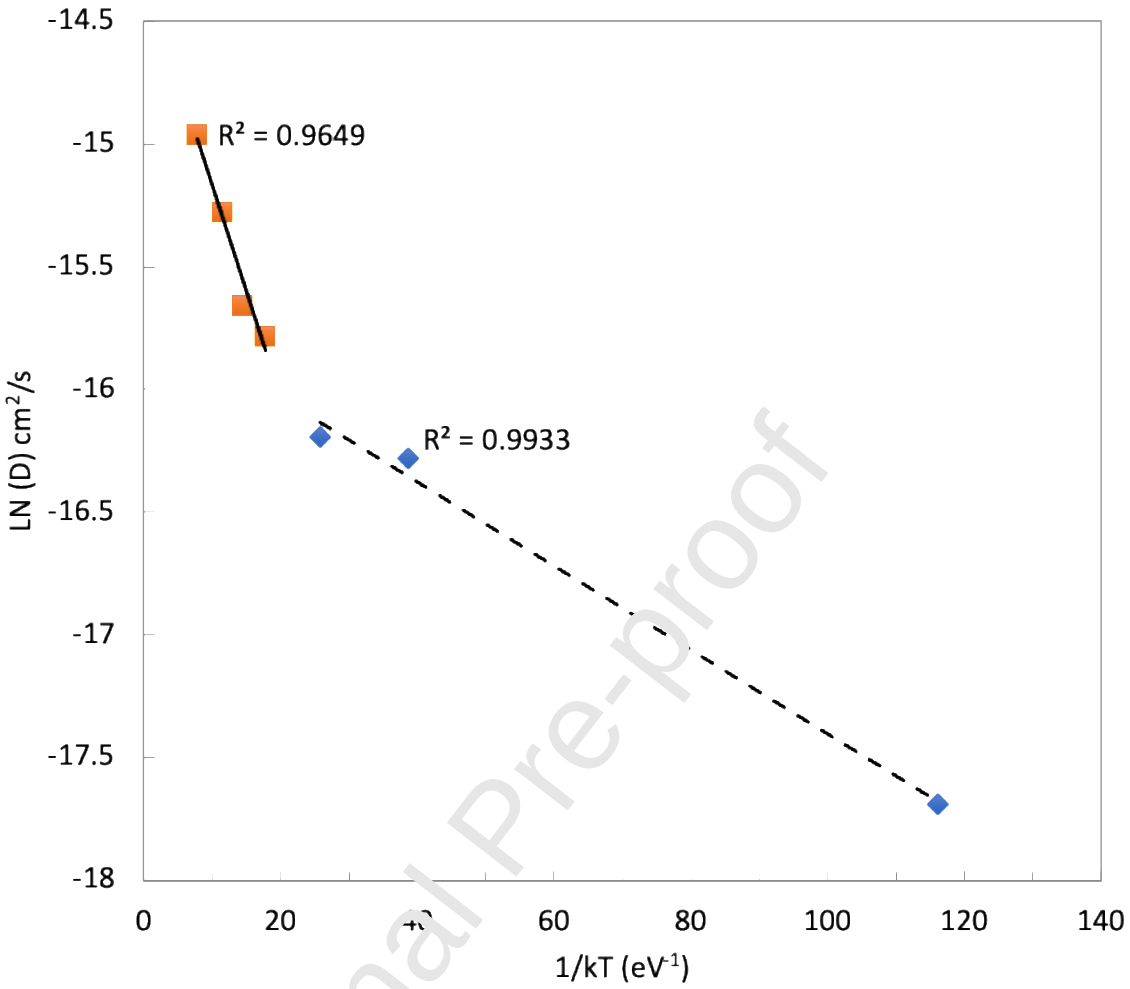

Figure 1: Arrhenius Plot of the diffusion coefficient (cm^2/s) as a function of 1/kT for the temperature range of 100-1500 K

3.2 Tracking Individual Hydrogen Motion: Intermittent Jumps

We investigated the displacement of each hydrogen atom as a function of temperature to examine the source of the two activation energy regions. As shown in Figure 2 and 3, instead of observing displacements for all hydrogen atoms in the system, only random atoms in the system have undergone displacement by the end of the simulation, the frequency of which increase as a function of temperature. For temperatures in the range of 100-450 K the majority

of the hydrogen atoms remain near their initial position throughout the simulation (Fig.1, region 1). However, as expected, as the temperature is increased atomic movement from the initial position increases substantially (Fig 1, region 2). For example, at 1500 K most hydrogen atoms in the system have undergone displacements from their original positions.

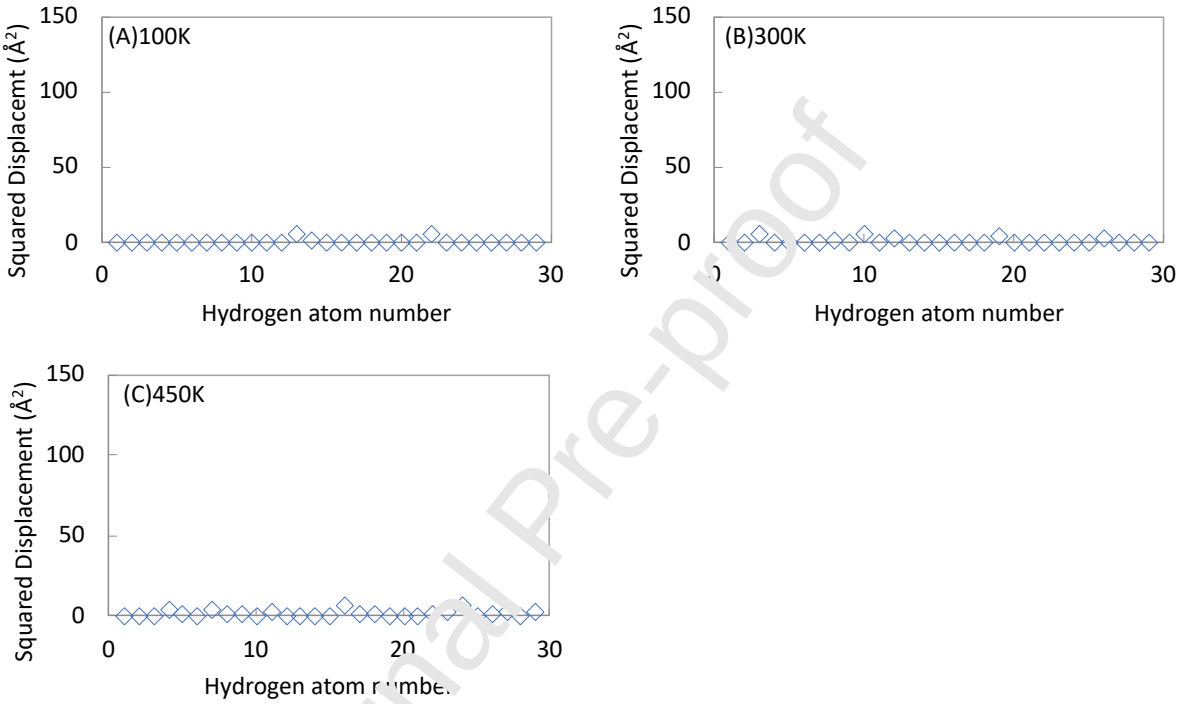

Figure 2: Mean squared displacement of a subset of hydrogen atoms in amorphous silica for the low activation energy region at 100 K (A), 300 K (B), and 450 K (C) after 2000 ps.

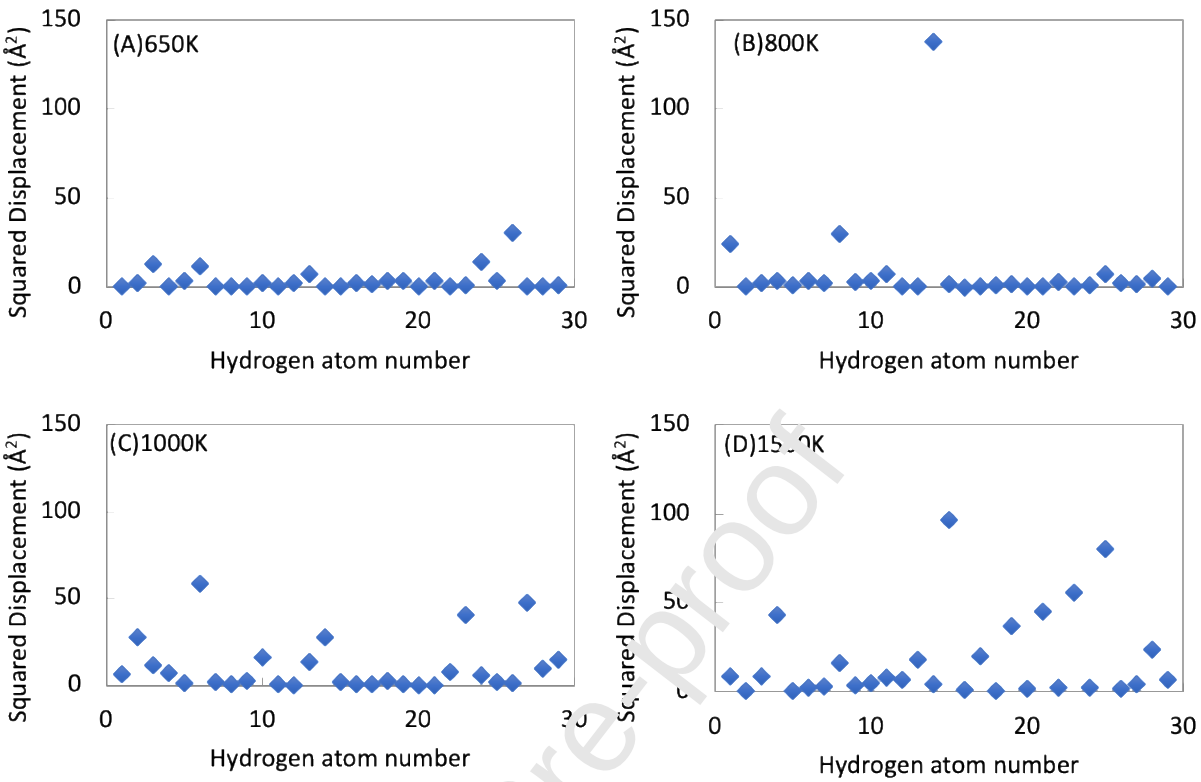

Figure 3: Atomic hydrogen mean squared displacement in amorphous silica for the high activation energy region at 650 K (A), 800 K (B), 1000 K (C), and 1500 K (D) after 2000 ps.

While Figures 2 and 3 show the net displacement of each atom, they do not elucidate the mechanism of displacement, nor can they account for the possibility of a hydrogen atom moving away from its initial position and then returning. By only tracking the displacement at the end of the simulation true atomic motion may be underestimated. Therefore, we also used MD to track individual hydrogen displacements as a function of simulation time for an even longer sampling duration, 4000 ps. As shown in Figure 4, instead of constant motion throughout the simulation, hydrogen atoms instead undergo intermittent jumps from one oxygen to another. For the first 400 ps the hydrogen atom is bonded to an oxygen atom and vibrates

around its initial site. It then undergoes its first jump to another oxygen site (as seen in the fluctuation region) where it again remains stable for another 2000 ps. In the final 1500 ps the hydrogen atom jumps two more times. The fluctuation bands in each region correspond to the hydrogen atom's local displacement when bonded to a specific oxygen atom. Figure 5 shows similar local atomic hydrogen displacements at about an oxygen atom at 1000 K. In the figure, the atomic hydrogen's fluctuations are confined to the Si-Si midplane, forming a cap-like shape around the oxygen atom. This migration continues until a jump occurs and a bond is formed with a new oxygen atom, resulting in another set of fluctuations and a second cap-like shape. Therefore, in contrast to the constant atomic motion observed in many other interstitial diffusion systems, the hydrogen atoms instead undergo intermittent jumps from one oxygen atom to another. A similar finding was reported by Godet et al. (2006) who used density functional theory to show this oxygen bonding state and demonstrate that cross-ring (from one oxygen atom to another across the plane) hydrogen jumps were more likely than nearest neighbor jumps. For solar wind implantation, atomic hydrogen diffusion via jumps from one oxygen atom to another also was also posited by Starukhina (2006) to describe the formation of metastable OH in lunar regolith. Findings from the present study support this O-to-O hopping diffusion mechanism throughout amorphous regolith.

We note that while bulk diffusion coefficients were used to examine hydrogen movement in lunar regolith (Starukhina, 2006; Farrell et al., 2015; 2017), the MD approach used in the current study reveals the detailed physical nature of the movement. Rather than being a continuous diffusive flow of H, the H atoms appear to move in abrupt stops-and-starts, with a

diffusion coefficient effectively integrating this impulsive movement across many H atoms to arrive at a bulk diffusion rate. The bulk rate does not reveal the underlying physical action (O-to-O jumps) that was initially described in Starukhina (2006) and clearly observed in the model herein.

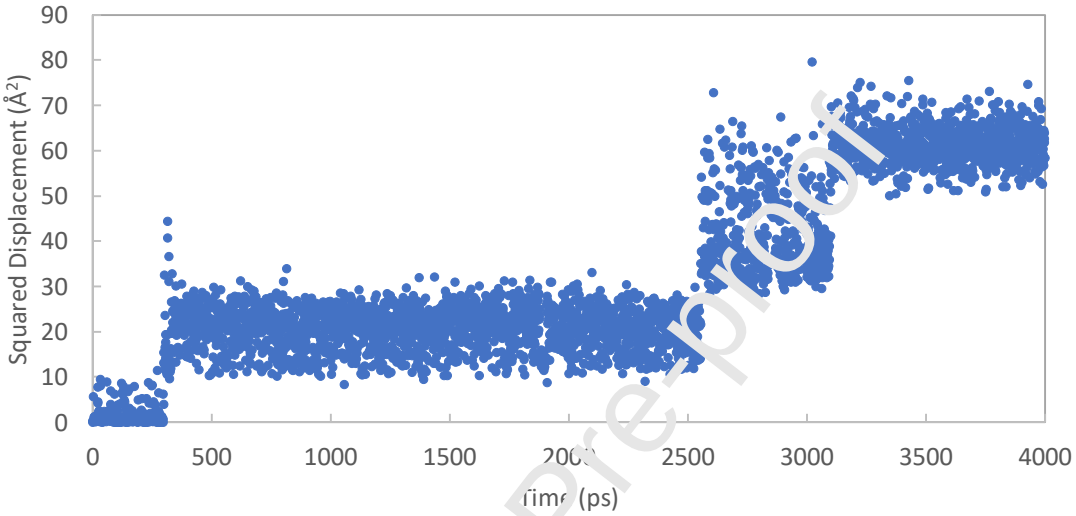

Figure 4: Squared displacement for an individual hydrogen atom at 1000 K in amorphous silica as a function of time showing three jumps.

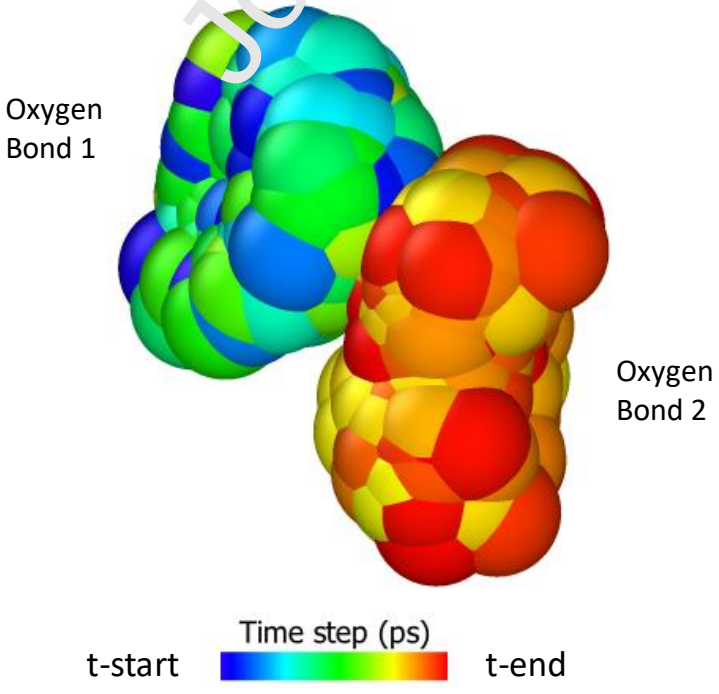

Figure 5: Position of a hydrogen atom at 1500 K as a function of time showing bonding with two different atoms over the simulation duration. The colors represent the position of the one hydrogen atom as a function of time.

A Python script was developed to track the number of and size of jumps for each hydrogen atom in the system over the total simulation time. A hydrogen jump was tracked by investigating the distance covered between each time step and correlating it with the individual MSD vs time plots as per Figure 4. In total, average jump distance for all temperatures (100-1500 K) was 3.4 Å with a standard deviation of $\pm$ 0.8 Å. This simulated jump size falls between previously simulated atomic hydrogen O-O hopping distances, 2.3-4.2 Å (Godet & Pasquarello 2006; Zhang et al. 2020). These simulated jumps were then used to calculate a normalized hydrogen jump rate as per equation 3:

$$Jump\ Rate_{normalized} = \frac{Total\ Number\ of\ H\ jumps}{Number\ of\ H\ atoms \times Simulation\ Duration} \qquad \text{Equation 3}$$

Figure 6 shows the normalized jump rates plotted as a function of temperature. With a given time and hydrogen concentration this normalized rate can be used to calculate the total number of hydrogen jumps at a specific temperature. As suggested by Figures 2-3, the normalized jump rate increased substantially with temperature (Figure 6).

These findings explain the appearance of the two activation energy regions observed in Figure 1. Previous research has suggested that displacements in the low activation energy

region (region 1) correspond to atomic vibrations only as opposed to diffusion throughout the bulk (Sheikholeslam et al. 2016). However, as per Figure 6, atomic hydrogen jumps from one oxygen to another, and thus diffusion, is still occurring within this region. In other words, while diffusion coefficients are low, there is displacement beyond just atomic vibrations around a single oxygen atom at low temperatures. Moreover, unlike Figure 1, when calculating the jump rate in Figure 6 we do not see an obvious transition in H atom motion at ~500K. Therefore, the appearance of two activation energy regions in Figure 1 is a related to the low temperature lattice vibrations influencing the diffusion coefficient. In contrast, at higher temperatures the jump rate is increased, and more widespread diffusion occurs throughout the lattice. As such, the activation energy in region 2 is less influenced by lattice vibrations and better represents actual diffusion. Given the intermittent nature of these jumps, this study highlights the importance of considering the motion of each individual atom as a function of the number of jumps, instead of solely considering the net mean square displacement or diffusion coefficient. Furthermore, depending on the temperature considered, simulations should model interactions for a suitable duration to ensure adequate statistical sampling of jumps.

We note that for solar wind implantation, the 1 keV proton typically implants to a depth of about 23 nm (230 Å) (Farrell et al. 2017). Therefore, the jump rate and average distance per jump can be combined to predict the maximum distance travelled by a hydrogen atom as a function of time. At 300 K, the subsequent jump probability of the hydrogen atom from Figure 6 is ~ 9 x 10^{-6}/ps. Extending this jump rate over 1 second, the number of expected jumps is then approximately 9 x 10^{6}, with each jump moving the hydrogen atom approximately ~3 Å. Thus,

the total distance the hydrogen atom travels via diffusion processes in 1 second at 300K is ~2.7 mm. Given that the surface is only 23 nm from the implantation site, some fraction of the implanted hydrogen at 300 K can diffuse to the surface and chemically combine with other regolith atoms and escape from the surface via combinative desorption processes that release products such as H_2, OH and H_2O into the exosphere (Starukhina 2006; Jones et al. 2018; Tucker et al. 2019). The silica modeled in our study is defect free and some fraction of the hydrogen atoms will also quickly migrate to deeper regions of the matrix. However, given the random walk of diffusion processes, we expect most of the implanted species to encounter the nearby surface in its migration. We do not consider the diffusion coefficient at 100K because no jumps were observed. Future work should include longer runs at these lower temperatures to obtain these jump rates.

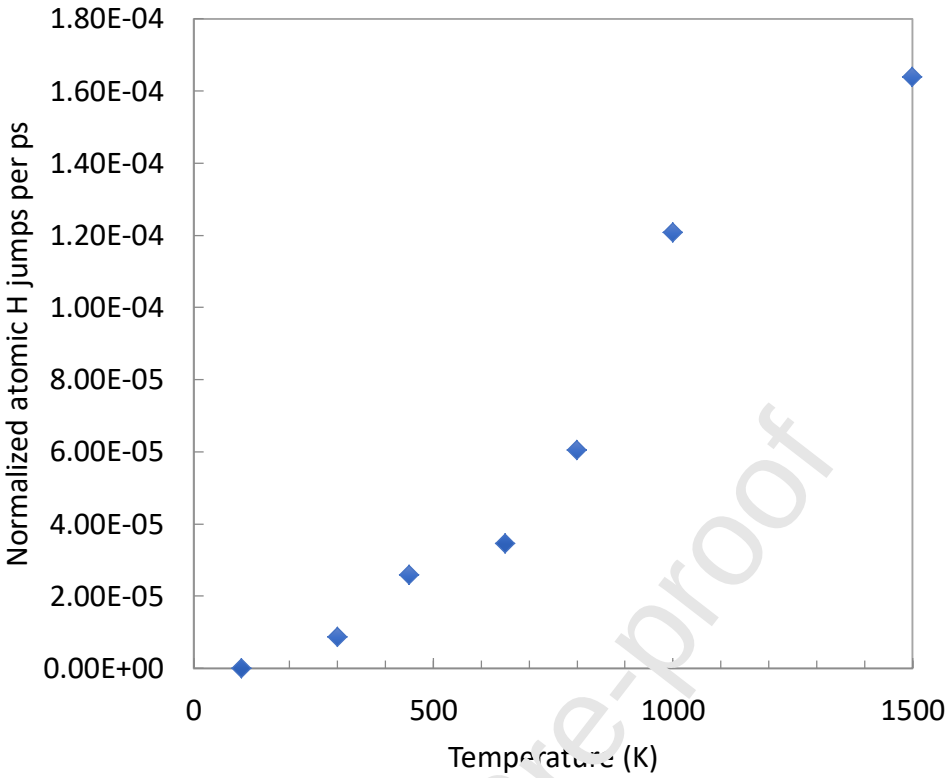

Figure 6: Normalized atomic hydrogen jumps (number jumps/total number hydrogen atoms) per picosecond as a function of simulation temperature.

3.3 Comparison to Simulation and Experiment

3.3.1 Diffusion Coefficient

Figure 7 compares the results of the MD simulations to a compilation of previous experimental and theoretical studies, the basis for this figure can be found in Fink et al. (1995). These experiments were conducted for H and on various silica arrangements including amorphous (vitreous) and irradiated. However, in contrast to atomistic simulations, experimental samples will inevitably contain several types of microstructural defects and traps including impurities, dislocations, and grain boundaries. Because MD simulations were

conducted using defect-free amorphous silica, they likely best represent the experimental results for H in vitreous silica.

Simulated diffusion coefficients in the present study increased from $9.0x10^{-8}$ to $3.2x10^{-7}$ cm^2/s as the simulation temperature was increased from 300 K to 1500 K. Previous MD simulations on atomic hydrogen diffusion in amorphous silica have predicted a wide range of possible diffusion coefficients. For example, Sheikholeslam et al. simulated for 200 ps and predicted a hydrogen atom diffusion coefficient of $1x10^{-11}$ cm^2/s at 650 K. However, the purpose of their study was to instead explain the role of strain on diffusion. In contrast Fogarty et al. used an identical potential and simulated for 600 ps, predicting an atomic hydrogen diffusion coefficient of $1.7x10^{-6}$ at 300 K. However, both these published diffusion coefficient results were discrepant by several orders of magnitude when compared to experimental diffusion coefficients for hydrogen atoms in amorphous silica (Figure 7). These previous studies were likely limited due to computational resource constraints, reducing the total simulation time that was conducted. In contrast, our MD results, which tracks MSD for a longer simulation time, predict a diffusion coefficient of $0.85x10^{-8}$ cm^2/s at 300 K, in better (qualitative) agreement with the experimental value of $1x10^{-7}$ cm^2/s (Figure 7). Qualitatively, we found the MD derived diffusion coefficients to be within the range of experimental results for hydrogen diffusion in various silica, though the slope remains discrepant. Our MD simulated diffusion coefficients, which used an identical interatomic potential and simulation set-up, differ from previous simulations because of the longer simulation and sampling durations. For shorter

simulated durations the statistical sample is potentially not large enough to capture the effect of intermittent jumps.

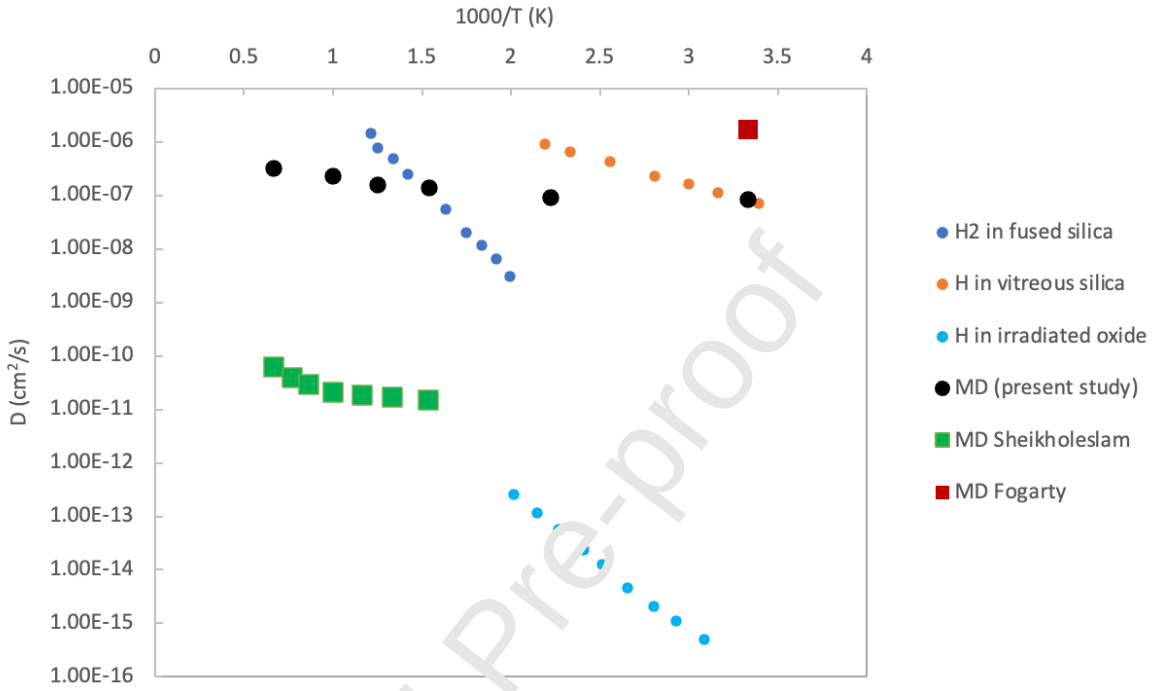

Figure 7: Experimental diffusion coefficient in silica compared to simulated diffusion coefficients from previous and present MD simulations (adapted from Fink et al. (1995)).

3.3.2 Activation Energy

Similar to the diffusion coefficient, there is also a large range in measured and simulated activation energies. Activation energies have been experimentally measured between 0.05 – 0.73 eV (Zhang et al. 2020), with Griscom et al. (1985) predicting an activation energy of 0.18 eV for atomic hydrogen in amorphous silica. In the low temperature region 1 our simulated activation energy was 0.02 eV, much lower than this experimental value. However, during the simulations diffusion in this region was limited and the activation energy was instead influenced

by lattice vibrations. In the higher temperature regions, our simulated activation energy for diffusion was 0.09eV, falling within the range of measured values for hydrogen in amorphous silica (0.05 – 0.73 eV). However, the MD simulations were carried out for an undamaged substrate which likely resulted in the predicted activation energies being lower than experiment for atomic hydrogen in vitreous silica.

4 Implications for Volatiles Implanted into Lunar Surfaces

4.1 Hydrogen Retention in Lunar Silicates

Findings from this study also have several important implications for volatiles implanted into lunar and planetary surfaces. As high energy hydrogen atoms impact the lunar surface they chemically react with oxygen in the regolith (SiO_2) to form various water products. However, there is a lack of knowledge on the extent to which diffusion can drive hydrogen migration and outgassing. These parameters are important for understanding the lifetime of implanted atomic hydrogen and subsequent water products. Lunar surfaces have a large range of possible temperatures depending both on location and time of day. For example, sunlight exposed surfaces can reach temperatures as high as 400 K, whereas at nightside or polar surfaces can fall below 100 K. An important finding of the present study is that hydrogen jumps, beyond just lattice vibrations, can occur in these temperature regions. Therefore, our study demonstrates that diffusion is present across both high and low lunar temperatures. Previous research by Starukhina (2006) supported a similar hydrogen jumping (from O to O) diffusion mechanism and agreed that diffusion rates were highly dependent on temperature .

However, while diffusion is occurring, the large range in jump rates and diffusion coefficients has important implications on the lifecycle of implanted volatiles. For example, diurnal variations in OH content as regions rotate into the warmer local noon were first suggested by Sunshine et al. (2009). In the present study, we demonstrate that for a temperature increase from 100 K to 450 K the diffusion coefficient increased by over 4 times. As per equation 4, the residence time (τ) can be expressed as a function of the activation energy (E), the diffusion constant (D_0)and the scale size (h):

$$\tau = h^2 \exp(\frac{-E}{T}) D_0^{-1} \quad \text{Equation 4}$$

Figure 8 compares the residence times for implanted hydrogen using results from the present study with experimental results for an activation energy of 0.5 eV for hydrogen in irradiated silica (Fink et al. 1995). In all cases a scale size of 100 nm was assumed. There is a clear difference in retention times for hydrogen in undamaged amorphous silica (the present MD results) as compared to experimental results for hydrogen in irradiated silica. At both high and low lunar temperatures the MD results predict a brief hydrogen retention in an undamaged amorphous silica. In contrast, as the activation energy is increased to that of irradiated silica, 0.5 eV (Fink et al. 1995), the retention time crosses the lunation boundary, leading to longer retention and a potential diurnal effect. Therefore, the retention times of SW implanted atomic hydrogen are highly dependent on the damage state of the silica substrate. Irradiated silica, which has a higher activation energy and retention time, has undergone extensive high energy impacts, likely leading to the formation of damage and defects within the substrate. This damage then leads to a subsequent increase in activation energy and the potential emergence of a diurnal effect. Specifically, as the lunar equatorial surface temperature varies from ~130K

at dawn to ~ 400K at noon, the surface with an activation energy near 0.5 eV goes from hydrogen-retentive (long retention times) in cool regions near the terminator to hydrogen emitting (short retention times) in warm regions close to local noon. This diurnal modulation is not expected for the regolith having a lower activation energy near 0.09 eV, since the hydrogen retention times are all relatively short. Future studies include creating a silica lattice with defects that mimic irradiated silica in order to study the effect on hydrogen diffusion.

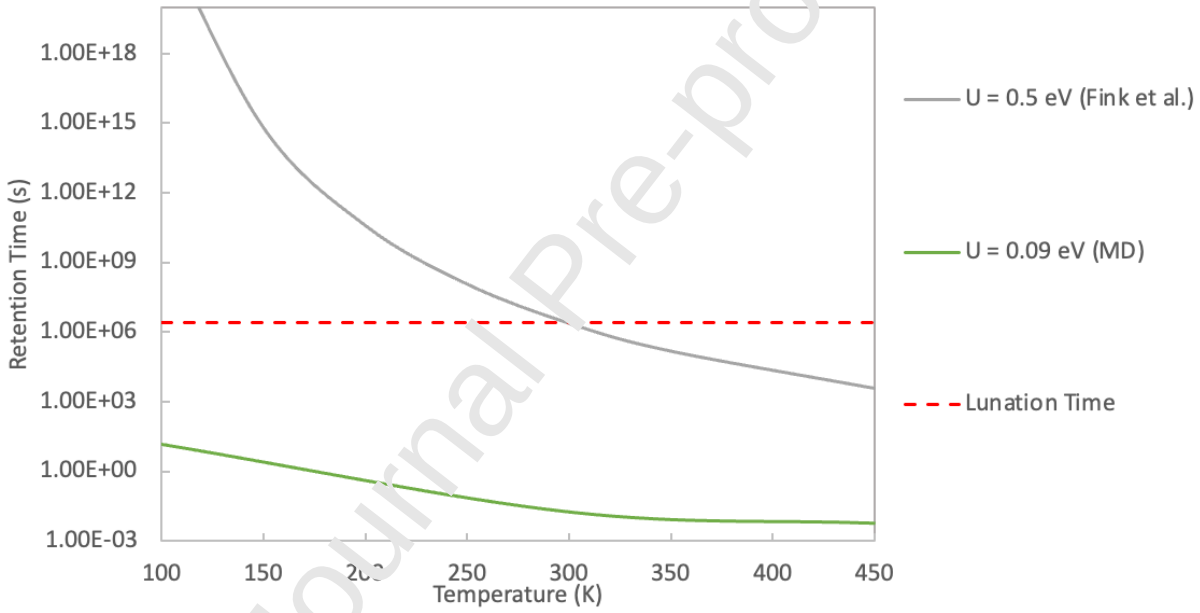

Figure 8: Residence time of implantation atomic hydrogen with temperature for various activation energies (adapted from Farrell et al. (2017))

4.2 Solar Wind Induced Damage: A Source of Trapping

The increased retention times for irradiated silica highlight the importance of considering damage and defects when modelling diffusion within a substrate. This process is particularly relevant for SW implantations which, in addition to depositing volatiles, can lead to lunar

surface weathering through the production of damage and defects in the grains. As such, we conducted simulations using both binary collision approximation (BCA) tools and MD to quantify the role of SW impacts in creating damage, which can potentially then trap implanted atomic hydrogen.

First, to quantify the role of SW impacts in creating damage we ran SDTrimSP simulations for 1 keV atomic hydrogen impacts onto an amorphous silica substrate at normal incidence. SDTrimSP is a BCA tool that is an extension of the Transport of Ions in Matter simulation tool (TRIM) (Mutzke et al. 2019). SDTrimSP can be run in standard (S) or dynamical mode (tracks compositional changes in the target substrate due to sputtering) using either serial (S) or parallel (P) processing on several computing operating systems. Damage was tracked using the Norgett−Robinson−Torrens displacements per atom (NRT-dpa) model as output in SDTrimSP (Mutzke et al. 2019). As seen in Figure 9, the implantation depth of SW atomic hydrogen peaked at 200 Å below the silica surface. The average number of displacements per incident hydrogen atom was 7.9, peaking at a depth of approximately 110 Å below the surface of the substrate. Therefore, the region of maximum damage occurs before the incoming projectile has settled into its maximum depth. Furthermore, approximately 60% of implanted hydrogen atoms are deposited between 110-250 Å. Over 50% of the total displacements created in the substrate occur within this depth region indicating damage is prevalent in the most probable implantation depth regions.

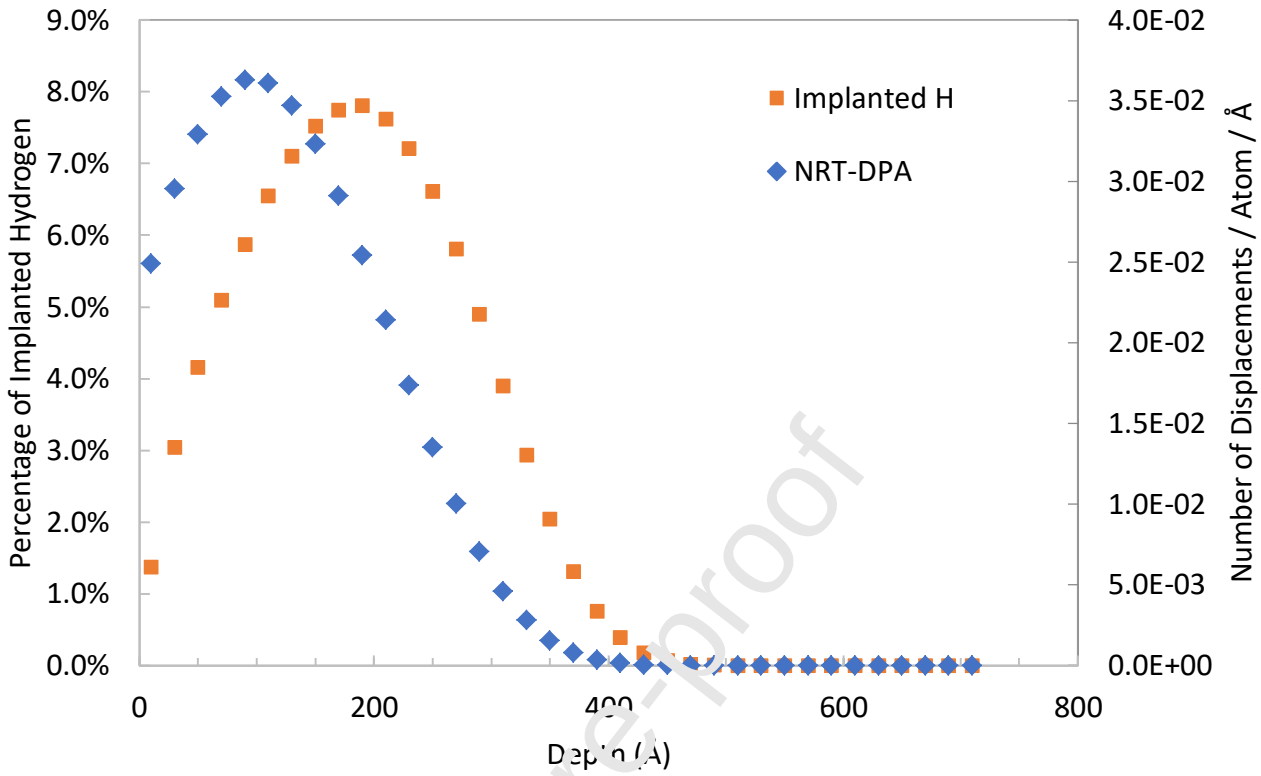

Figure 9: Percentage of implanted hydrogen (orange) (left vertical axis) and number of displacements (blue) (right vertical axis) as function depth for 1 keV hydrogen impacts onto an amorphous SiO_2 substrate using SDTrimSP.

As indicated in Figure 9, it is likely that implanted atomic hydrogen will interact with SW created defects within regolith particles. It is therefore important to understand whether these defects can potentially act as traps for implanted hydrogen, limiting diffusion and increasing the activation energy. To investigate potential defect trapping, additional MD simulations were run on a periodic amorphous silicate with a small spherical center void to simulate a defect as would be found in a damaged or weathered substrate. The substrate was prepared and equilibrated to 1000 K as per the methodology for the defect free silicates. This high temperature was chosen to simulate a regime where a high jump rate is expected in a defect

free amorphous sample. Seven hydrogen atoms were then deposited near the surface of the defect and the atomic motion was tracked as a function of time. As shown in Figure 10, after 2000 ps those atoms near the void have remained trapped to the void and have not undergone any displacement or jumps. In contrast, based on the jump rate calculated at 1000K, ~2 jumps would be expected in undamaged silica. Therefore, as expected, defects and voids likely have an important role in trapping atomic hydrogen and diffusion throughout the silica. Similar defect trapping of hydrogen has been observed in a number of other substrates (Myers et al. 1979; Picraux 1981; Islam et al. 2016). This trapping process likely explains the reduced diffusion and steeper slope observed for atomic hydrogen in an irradiated thermal oxide, e.g. Fink et al. [1995]) as compared to vitreous silica (Figure 7). As stated above, in future studies we will quantify the role of damage in increasing the activation energy and atomic hydrogen residence time.

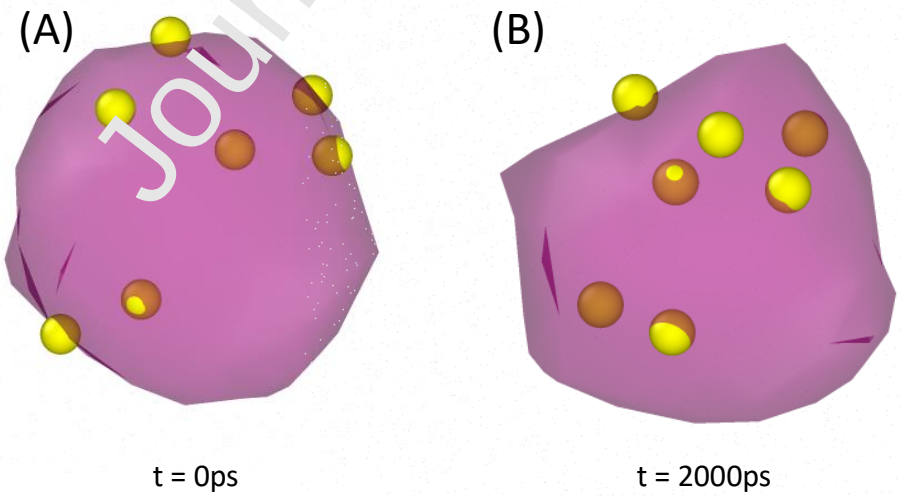

Figure 10: Hydrogen atoms (yellow) placed at the surface of a void (purple) within an amorphous silica at 1000 K at 0ps (A) and 2000ps (B). Silica atoms are not shown.

4.3 Solar Wind Induced Short Term Energy Spikes

The SW is also comprised of fractional higher mass ions such as helium, oxygen, and iron which are in higher proportion for the high energy tails (Von Steiger et al. 2000; Killen et al. 2012; Nénon & Poppe 2020). In addition to depositing volatiles and weathering the substrate, these incoming ions can deposit energy into the substrate leading to temporary localized thermal spikes (Tucker et al. 2005; Anders & Urbassek 2017). The radius of these temperature spike regions was approximately 7.5 Å for SW impacts onto ice (Anders & Urbassek 2017). As shown in the present study, atomic hydrogen movement in silica is highly dependent on temperature. For example, the solar wind flux at the subsolar point is approximately $2x10^{12}/m^2/s$ (Farrell et al. 2012; Poppe et al. 2018). At a sample time of 20 hours, this would lead to $1.4x10^{17}$ implantations/m^2. If the temperature spike was assumed to extend 7.5 Å in each direction, this would result in an affected 'spike' area of $7.1x10^{-18}$ m^2 for each impact. After only 10 hours of surface exposure the probability of an implanted atom being affected by a temperature spike is 10%. This increases to near 100% after 70 hours of exposure. Depending on expected retention time and deposition location, it is possible that implanted atoms can be driven by intermediate temperature spikes.

While diffusion of atomic hydrogen is occurring slowly at lunar temperatures, it may be increased by localized thermal spikes during proton impacts. The solar wind also contains a population of multi-charge massive ions (at the few percent level) (Poppe et al. 2018; Nénon & Poppe 2020) and the thermal spike areas associated these impacts are expected to be even larger in extent compared to proton impacts. Daytime exposed surfaces, which see a higher SW

flux than their nighttime or shadowed counterparts, are more likely to encounter localized spikes due to high energy SW impacts. For a temperature increase from 100 K to 1500 K, the high end of the simulated temperatures, the diffusion coefficient increased by over 15 times. Therefore, while overall exposed surface temperatures may not reach the high end of the temperatures simulated, localized spikes due to high energy SW impacts may be playing an important role in further driving the diffusion of atomic hydrogen in regolith. As shown in Figure 11, these increased diffusion rates increase the likelihood of atomic hydrogen diffusion to the surface, which is important to the subsequent degassing of hydrogenated molecules (Starukhina 2006). Therefore, SW may be at least partially responsible for two emission mechanisms, collisional sputtering during initial surface impacts, and increasing the probability of outgassing through temperature spikes, e.g. (Zeller et al. 1966)]. In a future study we will better constrain the probability of temperature spikes affecting implanted atoms by quantifying the radius, intensity, and durations of temperature spikes as a function of impacting atom type and energy.

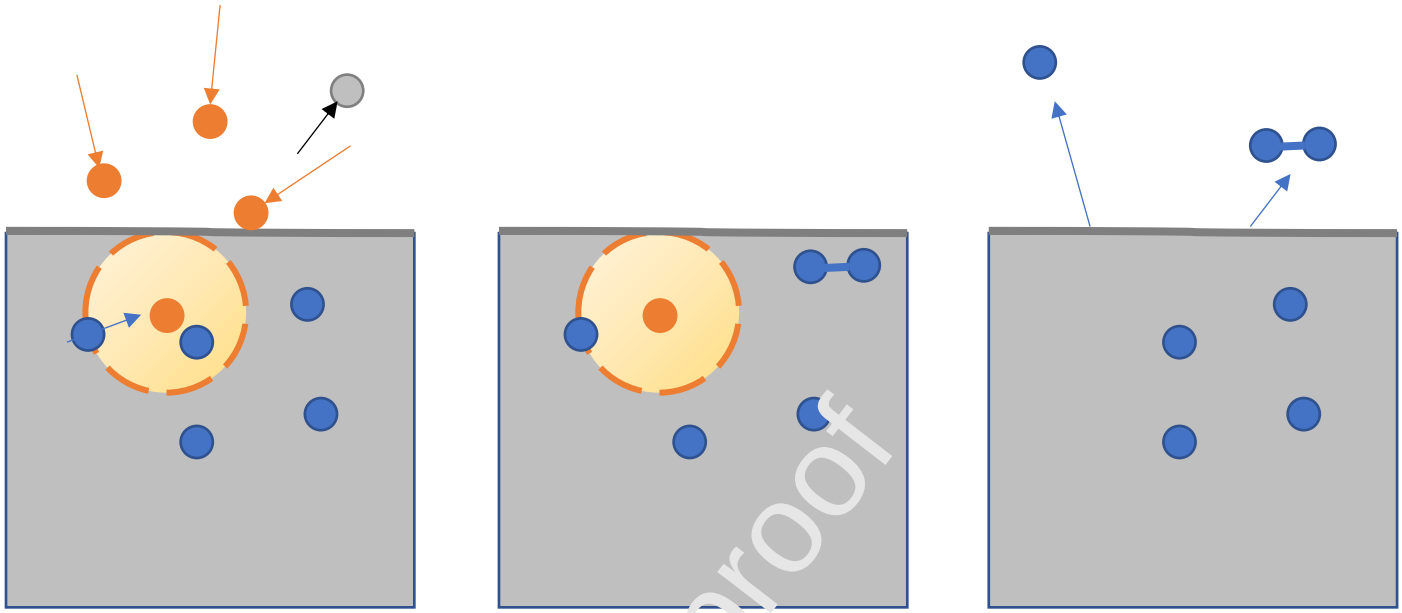

(A) SW impacts lead to sputtering and energy spike

(B) Spike drives diffusion, creating hydrogen molecule

(C) Hydrogen molecules and neutrals are outgassed

Figure 11: Illustration of the effect temporary energetic spikes driving diffusion and leading to outgassing of hydrogen. SW atoms are shown in orange, the silica substrate and sputtered atoms in grey, and implanted hydrogen atoms in blue

4.4 Applications to Lunar Magnetic Anomaly Regions

While the present MD simulations on undamaged amorphous silica likely overestimate the diffusive motion as compared to space weathered regolith grains, the simulations may have more relevance to freshly exposed regolith grains or magnetic anomaly regions that have undergone less space weathering (Farrell et al. 2017). Kramer et al. (2011) reported a reduced OH adsorption feature within lunar swirls as compared to other nearby regions. This reduction was attributed to the magnetic anomalies in these regions deflecting incoming SW ions. In these magnetic anomalies the solar wind energy and flux is can be reduced by over 80% due to

the ambipolar and Hall E field (Fatemi et al. 2015; Zimmerman et al. 2015; Poppe et al. 2016). Therefore, SDTrimSP simulations were also run for 200 eV hydrogen impacts onto an amorphous SiO_2 substrate. As per Figure 12, with a decrease in impact energy from 1 keV to 200 eV the average number of displacements per incident hydrogen atom decreased from 7.9 to 1.8, peaking at a depth of only 30 Å below the surface of the substrate. Therefore, a reduced impact energy leads to shallower deposits and less damage produced per impact. As qualitatively expected and quantified by the MD results, hydrogen diffusion is increased in substrates with less defects, which is expected in the shielded regions. Therefore, because magnetic anomaly regions have a decrease in damage production, our model calculations support the conclusion that the low surficial OH content found in lunar magnetic anomalies is in part due to a reduced diffusive lifespan of low energy implanted hydrogen.

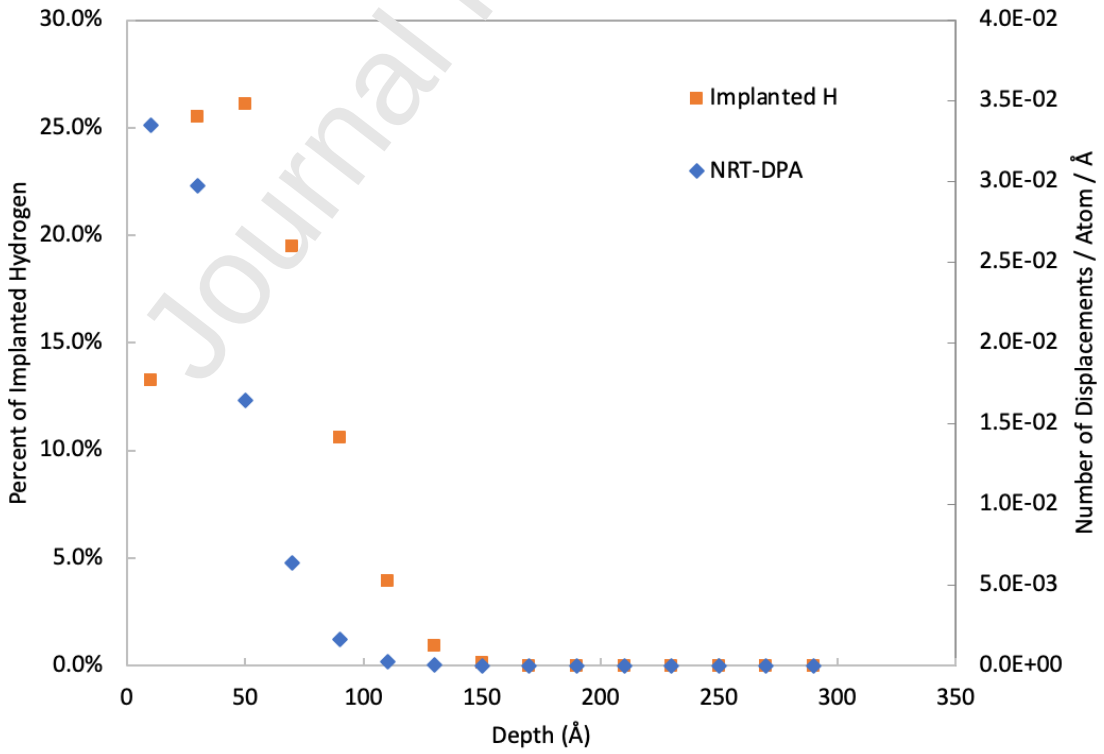

Figure 12: Percentage of implanted hydrogen (left vertical axis) and number of displacements (right vertical axis) as function depth for 200 eV hydrogen impacts onto an amorphous SiO_2 substrate using SDTrimSP.

5 Conclusions

We have performed baseline MD calculations of the diffusion of hydrogen atoms in amorphous silica as a function of temperature at the atomistic scale. Planetary scale models often adopt diffusion coefficients and activation energies from experiment or fit planetary data to examine phenomena such as the temporal variability of the lunar H_2O/OH veneer and subsequent degassing of water products to the lunar exosphere. Here we have shown how MD can be used to explicitly examine the effect of atomic level properties on diffusion to help further interpret both experimental and planetary data. Qualitatively, diffusion coefficients from the present study were more consistent with comparable experiments than previous MD simulations due to the use of longer simulation durations to increase statistics. A primary result from this study is that in contrast to the constant atomic motion observed in many other interstitial diffusion systems, the hydrogen atoms instead undergo intermittent jumps from one oxygen atom to another, the number of which increase with temperature. At lower temperatures most of the atomic motion was vibrations around a single oxygen atom, with jumps and thus diffusion being rare. As temperature was increased beyond 450 K there was notable increase in the frequency of oxygen to oxygen jumps leading to more hydrogen diffusion within the silica. Therefore, previously simulated low activation energies at low

temperatures are due to sampling of atomic vibrations instead of diffusion throughout the crystal.

From a planetary science perspective, the simulated low activation energy and jumps at lunar temperatures do not support the theory of diurnal variations in OH content for an undamaged amorphous silica surface. However, as damage from irradiation builds there is an increase in activation energy and the emergence of a potential diurnal variation. We conclude that energetic solar wind impacts can induce two competing atomic hydrogen motion processes in the exposed surface: 1) A prompt effect that induces jumps in the temperature spike volume, but 2) also a long-term effect of weathering and damage in the structure that acts to trap atomic hydrogen and increase retention. Exposure to the space environment makes the surface both self-trapping and self-releasing of the implanted species. To this end, it is critical for future MD examinations to examine the effects of the damage state of the substrate on hydrogen diffusion, retention, and subsequent water production, e.g. Tucker et al. (2019, 2021). This initial study has considered amorphous, defect-free, SiO_2 in order to compare with previous MD simulations and relevant experimental data. In a future study we will quantify how defects and more complex minerals affect the predicted activation energy for diffusion.

6 Acknowledgements

The material is based upon work supported by NASA under award number 80GSFC21M0002. Rosemary M. Killen, William M. Farrell, Orenthal J. Tucker, and Liam S. Morrissey were partially supported by the NASA Solar System Exploration Research Virtual Institute team LEADER.

7 References

Anders, C., & Urbassek, H. M. 2017, Icarus, 282, 351

Benna, M., Hurley, D. M., Stubbs, T. J., Mahaffy, P. R., & Elphic, R. C. 2019, Nat Geosci, 12, 333

Clark, R. N. 2009, Science (80-), 326, 562

Van Duin, A. C. T., Dasgupta, S., Lorant, F., & Goddard, W. A. 2001, J Phys Chem A, 105, 9396

Elphic, R. C., Funsten III, H. O., Barraclough, B. L., et al. 1991, Geophys Res Lett, 18, 2165

Farrell, W. M., Halekas, J. S., Killen, R. M., et al. 2012, J Geophys Res Planets, 117

Farrell, W. M., Hurley, D. M., Esposito, V. J., McLain, J. L., & Zimmerman, M. I. 2017, J Geophys Res Planets, 122, 269

Farrell, W. M., Hurley, D. M., & Zimmerman, M. I. 2015, Icarus, 255, 116

Fatemi, S., Lue, C., Holmström, M., et al. 2015, J Geophys Res Sp Phys, 120, 4719

Feldman, W. C., Maurice, S., Binder, A. B., et al. 1998, Science (80-), 281, 1496

Fink, D., Krauser, J., Nagengast, D., et al. 1995, Appl Phys A, 61, 381

Fogarty, J. C., Aktulga, H. M., Grama, A. Y., Van Duin, A. C. T., & Pandit, S. A. 2010, J Chem Phys, 132, 174704

Godet, J., & Pasquarello, A. 2006, Phys Rev Lett, 97, 155901

Griscom, D. L. 1985, J Appl Phys, 58, 2524

Haynes, W. M. 2014, CRC handbook of chemistry and physics, CRC press)

Islam, M. M., Zou, C., van Duin, A. C. T., & Raman, S. 2016, Phys Chem Chem Phys, 18, 761

Jones, B. M., Aleksandrov, A., Hibbitts, K., Dyar, M. D., & Orlando, T. M. 2018, Geophys Res Lett, 45, 10

Kallio, E., Dyadechkin, S., Wurz, P., & Khodachenko, M. 2019, Planet Space Sci, 166, 9

Killen, R. M., Hurley, D. M., & Farrell, W. M. 2012, J Geophys Res Planets, 117

Killen, R. M., & Ip, W. 1999, Rev Geophys, 37, 361

Kramer, G. Y., Besse, S., Dhingra, D., et al. 2011, J Geophys Res Planets, 116

Mattern, P. L., Thomas, G. J., & Bauer, W. 1976, J Vac Sci Technol, 13, 430

McCord, T. B., Taylor, L. A., Combe, J., et al. 2011, J Geophys Res Planets, 116

McKay, D. S., Heiken, G., Basu, A., et al. 1991, Lunar Sourceb, 567, 285

Mutzke, A., Schneider, R., Eckstein, W., et al. 2019

Myers, S. M., Picraux, S. T., & Stoltz, R. E. 1979, J Appl Phys, 50, 5710

Nénon, Q., & Poppe, A. R. 2020, Planet Sci J, 1, 69

Picraux, S. T. 1981, Nucl Instruments Methods, 182, 413

Pieters, C. M., Goswami, J. N., Clark, R. N., et al. 2009, Science (80-), 326, 568

Plimpton, S. J. 1995, J Comput Phys, 117, 1

Poppe, A. R., Farrell, W. M., & Halekas, J. S. 2018, J Geophys Res Planets, 123, 37

Poppe, A. R., Fatemi, S., Garrick-Bethell, I., Hemingway, D., & Holmström, M. 2016, Icarus, 266, 261

Saal, A. E., Hauri, E. H., Cascio, M. L., et al. 2008, Nature, 454, 192

Sarantos, M., & Tsavachidis, S. 2020, Geophys Res Lett, 47, e2020GL088930

Schultz, P. H., Hermalyn, B., Colaprete, A., et al. 2010, Science (80-), 330, 468

Sheikholeslam, S. A., Manzano, H., Grecu, C., & Ivanov, A. 2016, J Mater Chem C, 4, 8104

Starukhina, L. V. 2006, Adv Sp Res, 37, 50

Starukhina, L. V, & Shkuratov, Y. G. 2000, Icarus, 147, 585

Von Steiger, R., Schwadron, N. A., Fisk, L. A., et al. 2000, J Geophys Res Sp Phys, 105, 27217

Stern, S. A., Cook, J. C., Chaufray, J.-Y., et al. 2013, Icarus, 226, 1210

Sunshine, J. M., Farnham, T. L., Feaga, L. M., et al. 2009, Science (80-), 326, 565

Tucker, O. J., Farrell, W. M., Killen, R. M., & Hurley, D. M. 2019, J Geophys Res Planets, 124, 278

Tucker, O. J., Farrell, W. M., & Poppe, A. R. 2021, J Geophys Res Planets, 126, e2020JE006552

Tucker, O. J., Ivanov, D. S., Zhigilei, L. V, Johnson, R. E., & Bringa, E. M. 2005, Nucl Instruments Methods Phys Res Sect B Beam Interact with Mater Atoms, 228, 163

Williams, R. J., & Jadwick, J. J. 1980, NASA Ref Publ Ser

Zeller, E. J., Ronca, L. B., & Levy, P. W. 1966, J Geophys Res, 71, 4855

Zhai, D., Zhao, L., Gao, J., & Xu, C. 2012, Phys Chem Chem Phys, 14, 7296

Zhang, F.-J., Zhou, B.-H., Liu, X., Song, Y., & Zuo, X. 2020, Chinese Phys B, 29, 27101

Zimmerman, M. I., Farrell, W. M., & Poppe, A. R. 2015, J Geophys Res Planets, 120, 1893

Highlights

- H atoms undergo intermittent jumps from one O atom to another
- Number of H jumps increases with temperature
- Diffusion coefficients had better agreement to experiment than past MD simulations
- SW induces two competing atomic hydrogen motion processes in the exposed surface
- Damage is dependent on impact energy
- Defects easily retain implanted hydrogen